

Cite this: *Mater. Adv.*, 2026,  
7, 2311

# The influence of carbon nanotubes on the abrasion and crack growth behaviors of styrene–butadiene rubber compounds

Gi-Bbeum Lee,<sup>a</sup> Eun Jung Han,<sup>a</sup> Dawon Kang,<sup>a</sup> Preeyanuch Junkong<sup>id</sup><sup>c</sup> and Changwoon Nah<sup>id</sup><sup>\*abc</sup>

In this study, the influence of carbon nanotubes (CNTs) on the wear and crack growth behaviors of styrene–butadiene rubber (SBR) vulcanizates was reported. Two types of carbon black (CB)-filled SBR compounds were prepared with a total filler loading of 50 phr. In each case, a small fraction (~3 phr) of CB was replaced either with pristine CNTs (p-CNTs) or with surface-modified CNTs (T-CNTs). The surface modification of CNTs was carried out using a silane coupling agent (Si-69). Wear resistance and crack growth behaviors were evaluated by using a blade-type abrader and a dynamic fatigue instrument, respectively. The SBR-containing p-CNT exhibited reduced wear resistance, as the unmodified CNT was more easily pulled out by the blade during abrasion. On the other hand, the SBR containing T-CNTs demonstrated improved wear resistance (1 phr of T-CNT: 6–7.5% improvement), attributed to the enhanced interaction between the CNTs and the SBR matrix facilitated by the silane coupling agent, which reduced the amount of CNT pull-out. Crack growth resistance was improved in both SBR containing p-CNTs (7.1–60.6% improvement) and T-CNTs (39.8–71.8% improvement). This enhancement is explained by the gradual and partial pull-out of CNTs under repeated straining, which contributed to energy dissipation and improved fatigue resistance, even in the absence of surface modification.

Received 16th October 2025,  
Accepted 7th January 2026

DOI: 10.1039/d5ma01175b

rsc.li/materials-advances

## 1. Introduction

Rubber materials are used in various fields such as automobiles, shoes, aerospace, electronic devices, medical devices, and sporting goods due to their unique viscoelastic properties, such as high elasticity and high stretchability.<sup>1,2</sup> Among these applications, the tire industry represents the largest consumer of rubber materials, accounting for more than 75% of global rubber consumption.<sup>3</sup> Styrene–butadiene rubber (SBR), one of the most commonly used synthetic rubbers, is a copolymer made by polymerizing butadiene and styrene, and is widely used in the tire industry due to its excellent abrasion resistance, traction properties, and rolling resistance.<sup>4,5</sup> In particular, solution-polymerized SBR provides low hysteresis and offers the advantage of precise control over the chain-end structure, molecular weight distribution, and butadiene microstructure,

making it useful in tire compounds.<sup>6–8</sup> Furthermore, to enhance the performance of SBR for tire applications, reinforcing fillers such as carbon black (CB) and silica are commonly incorporated into the rubber matrix.<sup>6,7,9–12</sup>

Two mechanical properties are particularly critical in tire applications: wear resistance, which governs wear life during road contact, and fatigue resistance, which determines the durability of the compound under repeated cyclic deformation. Since these properties are directly related to the stability and lifespan of tires, the rubber compound with higher wear resistance and fatigue resistance should be considered in tire applications. These properties are strongly influenced by the filler type, filler dispersion, polymer–filler interactions, cross-link density, and network morphology,<sup>7,8,11–13</sup> and extensive research has been carried out to enhance them.

The functional modification of SBR is one effective approach to improve filler dispersion and polymer–filler interaction. Thielen *et al.* studied the functionalized emulsion SBR with hydroxypropyl methacrylate (HPMA) as a polar group.<sup>14</sup> HPMA exhibited strong compatibility with the silanol groups on the silica surface, enhancing silica dispersion and consequently improving the wear resistance of the silica-filled SBR compound. Kim *et al.* selected glycidyl methacrylate (GMA) as a

<sup>a</sup> Department of Bio-Nanotechnology and Bioconvergence Engineering, Jeonbuk National University, Jeonju, 54896, Korea. E-mail: cnah@jbnu.ac.kr

<sup>b</sup> Polymer-Nano Science and Technology, Jeonbuk National University, Jeonju, 54896, Korea

<sup>c</sup> Department of Chemistry, Faculty of Science, Mahidol University, Nakhon Pathom, 73170, Thailand



third monomer to improve compatibility with silica.<sup>15</sup> Functionalization with GMA allowed the silica-filled SBR compound to achieve a 32.9% increase in wear resistance. Seo *et al.* synthesized acrylonitrile–styrene–butadiene rubber (AN-SBR), in which the polar monomer acrylonitrile (AN) was introduced as a third monomer into emulsion SBR, and applied it to a silica compound.<sup>16</sup> The wear resistance of the silica compound containing AN-SBR increased by approximately 14%, due to enhanced hydrogen bonding between the nitrile groups of acrylonitrile and the silanol groups on the silica surface, which strengthened the rubber–filler interaction.

Modification of fillers is another method to increase polymer–filler interaction and improve filler dispersion in the rubber matrix. Torbati-Fard *et al.* studied the effects of silica surface modification by low-molecular-weight hydroxyl-terminated polybutadiene (HTPB) and bis(3-triethoxysilylpropyl)tetrasulfide (TESPT).<sup>17</sup> Both TESPT and HTPB are capable of chemical bondings to silica and rubber, thereby strengthening the rubber–filler interactions and consequently improving the dispersion in the SBR compound. This enhancement in dispersion was reflected in the improved wear resistance. The greater steric hindrance of HTPB leads to better nanometric dispersion of silica. However, the SBR compound containing TESPT-modified silica demonstrates higher wear resistance. This enhancement is attributed to the rigid interfacial bonding between SBR and silica by TESPT. Liang *et al.* developed a method to modify the surface of carbon black (CB) through hydroxylation and silane coupling, which enhances its dispersion and consequently improves the mechanical performance of rubber compounds.<sup>18</sup> CB was initially treated using a modified Hummers oxidation method, followed by the conversion of oxygen-containing functional groups into hydroxyl groups. Subsequently, the surface of the pre-modified CB was further functionalized with the organo-silane coupling agent, KH-570. This promotes the dispersion of CB and the rubber–filler interfacial strength, resulting in an increase in wear resistance of approximately 18%.

The styrene content of SBR is one of the factors influencing various mechanical properties of SBR compounds. Um *et al.* investigated the influence of styrene content of solution SBR (SSBR) on both silica dispersion and tire tread performance.<sup>8</sup> As the styrene content in SSBR increased, silica dispersion and rubber–filler interactions in SBR compounds improved due to the rigid and electron-rich aromatic styrene groups, which inhibited silica agglomeration. By the same mechanism, wear resistance was also enhanced. Wang *et al.* studied the effect of the styrene content in SBR and its interaction with CB on the dynamic fatigue performance of the SBR compound.<sup>19</sup> Since both the filler network formed by CB and the styrene increase the rigidity of the SBR compound, the energy required for crack growth is increased, thereby reducing the crack propagation rate. Consequently, as the styrene content in SBR increases, the dynamic fatigue life of the SBR composite is prolonged.

Recently, studies have proposed hybrid filler systems employing two or more fillers to enhance the wear resistance and fatigue resistance of rubber compounds. Thaptong *et al.*

investigated the effect of the ratio of highly dispersible silica to CB hybrid fillers in SSBR-based tire treads.<sup>20</sup> The wear resistance increased as the CB ratio rose, possibly due to the reduced amount of mobilized rubber and the lower friction coefficient of the vulcanizates at higher CB contents. The wear resistance was highest when the CB ratio was 80%, while a CB ratio of 40% provided the best balance of tire performance, including wear resistance, wet grip, and fuel-saving efficiency. Numerous studies have focused on hybrid filler systems in SBR compounds, in which CB or silica is partially replaced by CNTs, graphene, clay, and other similar nano-materials. These fiber- or sheet-like fillers can provide a significant reinforcement even at low loadings due to their high aspect ratios. Mazumder *et al.* investigated the effects of hybrid filler systems incorporating organically modified nanoclay (ONC) and exfoliated graphene nanoplatelets (xGNP) in silica-filled SBR/BR compounds.<sup>21</sup> In the hybrid filler compounds, silica was partially replaced by 1, 2, 3, and 5 phr of ONC or xGNP. The increase in nanoclay and graphene contents enhanced rubber–filler interactions due to their high aspect ratios, leading to improvement in both wear resistance and fatigue resistance. The wear resistance was more significantly improved in hybrid filler compounds containing nanoclay, whereas the fatigue resistance was more pronounced in those containing graphene. Dolui *et al.* studied the synergistic effect of hybrid filler systems, *viz.*, graphene oxide/silica (GO/SiO<sub>2</sub>), CNT/silica (CNT/SiO<sub>2</sub>), and graphene oxide/CNT/silica (GO/CNT/SiO) on hydrogenated SBR compounds.<sup>22</sup> Silica was replaced by 3 phr of GO, CNTs, or a 1 : 1 blend of GO/CNT. The wear resistance of the GO/SiO<sub>2</sub>, CNT/SiO<sub>2</sub>, and GO/CNT/SiO<sub>2</sub> hybrid filler compounds increased by up to 39%, 75%, and 87%, respectively. This improvement in wear resistance is attributed to the enhanced rubber–filler interactions provided by GO and CNTs. In particular, in the case of the CNT, this effect appears to be more pronounced due to its higher stiffness and aspect ratio. On the other hand, the fatigue resistance of all hybrid filler compounds decreased slightly. Yin *et al.* investigated the effect of aramid fibers (AFs) on the crack growth of CB-filled SBR composites.<sup>23</sup> The crack growth rate of the CB-filled SBR composite containing 2 phr of AF coated with butadiene–vinyl pyridine copolymer latex (VPL) decreased, resulting in improved fatigue resistance. When a propagating fatigue crack encounters the fibre-shaped AF, the crack propagation direction changes along the fibre, creating a more complex crack growth contour, leading to a reduction in the crack growth rate. In addition, the flexible interface formed by the VPL prevents excessive damage to the matrix rubber, further decreasing the crack growth rate. Kodal *et al.* studied the influence of CNTs on the performance of CB-filled NR/SBR tire compounds.<sup>24</sup> In the NR/SBR/CB compound containing 10 phr of CNT, the CNT particles were uniformly dispersed, increasing the available surface area for interaction between the rubber matrix and the fillers. As a result, the wear resistance was enhanced. Rhue *et al.* investigated the effects of partial replacement of CB with CNTs in the SBR/BR/CB/CNT compound.<sup>25</sup> The wear resistance of the compound, in which CB was partially replaced by 6–7.75 phr of CNT, was improved, and the effect was more pronounced when sulfur-functionalized



CNTs were used. The enhancement in wear resistance is attributed to the increased stiffness and strength of the compound due to CNT addition, while the additional improvement is considered to result from the enhanced dispersion of CNTs and the stronger rubber–filler interaction provided by sulfur functionalization.

The wear of rubber materials arises from the combined action of multiple mechanisms, including cutting, shear, impact, adhesive, fatigue, and thermal or oxidative processes, which makes the precise identification of the wear mechanisms challenging.<sup>26,27</sup> Various wear testing methods have been developed to predict the wear characteristics of rubber materials. Representative methods include the cut and chip (CC) test, Lambourn test, DIN abrasion test, LAT100, and the blade-type wear tester.<sup>28–32</sup> Fatigue failure of rubber materials refers to the phenomenon in which the strength of the rubber gradually deteriorates under repeated loading, eventually leading to failure. To evaluate the fatigue resistance of rubber materials, two main approaches are commonly employed: (i) predicting fatigue life based on the number of applied strain cycles to failure and the corresponding strain energy density,<sup>33–35</sup> and (ii) assessing fatigue resistance by measuring the crack growth rate as a function of tearing energy under cyclic loading.<sup>36,37</sup> The wear and fatigue properties of rubber compounds may slightly differ, depending on the testing methods used, as each method involves variations in specimen geometry, load, temperature, speed, and other testing conditions. In the case of wear properties, even the same rubber compound exhibited different abrasion resistance depending on the wear tester employed.<sup>30</sup> Therefore, a comprehensive understanding of wear and fatigue mechanisms across various testing methods is essential for the rational design of high-performance rubber compounds.

While previous studies have explored the effects of hybrid filler systems on the wear and fatigue properties of SBR compounds, the specific influence of a hybrid filler system composed of CB and silane-modified CNTs remains unexplored. Furthermore, to our knowledge, no studies have investigated the wear behavior of such SBR compounds using a blade-type wear tester.

In this study, in order to examine the effects of the content and surface modification of the CNT, a fiber-shaped filler, on the characteristics of wear and fatigue fracture of rubber compounds, specimens were made by adding CB and CNTs to SBR, and the wear resistance and fatigue resistance were evaluated separately. A solution-polymerized SBR, a commercially widely accepted rubber in the tire industry, was employed. For carbon black (CB), N134, which has a small particle size and a high degree of structure (Fig. S1 and Table S1), was selected, as the SBR compound filled with N134 exhibited the highest wear resistance compared to compounds with other types of CB (Fig. S2). The surface modification of CNTs was performed using a silane coupling agent (Si-69), and the content of the filler was adjusted by replacing CB with a small amount of CNT, with CB 50 phr as the standard. To prevent additional variables arising from poor dispersion of CB and to more accurately assess the intrinsic influence of the CNT, the total content of the filler was set

to 50 phr. The wear performance was evaluated using a blade-type wear tester equipped with a zirconia blade, and the fatigue fracture performance was evaluated using a self-made dynamic fatigue fracture tester.

Through a systematic investigation of these factors, this study is expected to provide guidance for designing tire materials with high wear and fatigue resistance through the effective incorporation of CNTs and their surface modification in CB-filled SBR compounds.

## 2. Experimental

### 2.1. Materials

Styrene–butadiene rubber (SBR) used was SOL 6361H (solution-polymerized SBR, styrene content: 33 wt%, vinyl content: 58 wt%) from the Kumho Petrochemical Co. Carbon black (N134, diameter = 20–25 nm, OCI Company Ltd) and carbon nanotube (CM280, diameter = 10–20 nm, length = 200–250 μm, Hanwha Chemical Co.) were used as fillers. Sulfur (Samchun Pure Chemical Co.) was used as a crosslinking agent, zinc oxide (ZnO, Sigma-Aldrich) and stearic acid (S/A, Sigma-Aldrich) were used as crosslinking activators, *N-tert*-butyl benzothiazol-2 sulfenamide (NS, Sigma-Aldrich) was used as a crosslinking accelerator, and Irganox 1010 (Sigma-Aldrich) was used as an antioxidant. Sulfuric acid (98% H<sub>2</sub>SO<sub>4</sub>, Sigma-Aldrich), nitric acid (60% HNO<sub>3</sub>, Samchun Pure Chemical Co.), and the silane coupling agent (Si-69) were used to modify the surface of carbon nanotubes. Toluene (≥ 99.5%, Samchun Pure Chemical Co.) and methanol (≥ 99.5%, Samchun Pure Chemical Co.) were used as solvents for the modification of CNTs.

### 2.2. Modification of carbon nanotubes (CNTs)

The surface modification of CNTs was performed in two steps: the first step was to generate OH groups on the CNT surface, and the second step was to make the generated OH groups react with a silane coupling agent (Si-69) (Fig. 1). 0.25 g of CNTs and 250 ml of a mixture of nitric acid and sulfuric acid (1 : 3 in volume ratio) were added to a beaker, followed by ultrasonic treatment for 3 h and washing with deionized (DI) water until the pH reached 7. The washed mixture was vacuum filtered

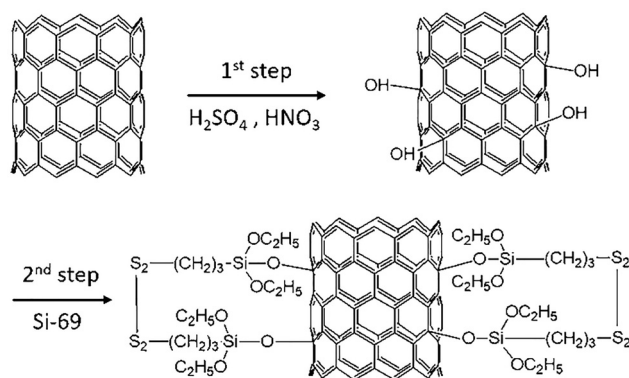


Fig. 1 Modification of CNTs with H<sub>2</sub>SO<sub>4</sub>, HNO<sub>3</sub>, and the silane coupling agent (Si-69).



using a membrane filter (cellulose acetate, pore size: 0.2  $\mu\text{m}$ ) and dried in a vacuum oven at 50  $^{\circ}\text{C}$  for 48 h to produce CNTs surface-modified with OH groups (step 1). 0.25 g of CNTs surface-modified with OH groups and 100 ml of toluene were added to a beaker and sonicated for 10 min. 2 ml of a silane coupling agent (the weight ratio, CNT:Si-69 = 1:8) was added and stirred at 75  $^{\circ}\text{C}$  and 150 rpm for 6 h. The mixture was then washed with methanol, and the mixture was vacuum filtered using a membrane filter (cellulose acetate, pore size: 0.2  $\mu\text{m}$ ) and dried in a vacuum oven at room temperature for 24 h (step 2). The CNT finally modified with the silane coupling agent was named T-CNT.

### 2.3. Preparation of rubber compounds

The composition of the rubber compound used in this experiment is shown in Table 1. The content of the filler was initially set at 50 phr of CB, and subsequently prepared by partially replacing CB with a small amount of CNT. SBR was masticated in a Banbury mixer (Namyang Enterprise Co., Ltd, Korea) for 1 min at 150  $^{\circ}\text{C}$  and 50 rpm. Then, the filler, Irganox 1010, ZnO, and S/A were added sequentially, and the master batch was mixed for 3, 1, and 2 min, respectively. The final compound was prepared by adding crosslinking agents into the master batch, followed by additional mixing for 10 min using a two-roll mill (DS-1500R, WITHLAB Co. Ltd, Korea). The optimum curing time ( $T_{90}$ ) of the compound was measured at 170  $^{\circ}\text{C}$  using an oscillating rheometer (ODR, Alpha Technology, USA). Specimens were subsequently crosslinked by compression of 10 tons at 170  $^{\circ}\text{C}$  using a hydraulic press (CMV50H-15-CLPX, Carver, Inc., USA). For evaluation of fatigue fracture characteristics and mechanical properties, specimens were crosslinked into a sheet for the duration of  $T_{90}$ , whereas specimens for wear testing were molded in a cylinder shape and cured for the optimum cure time.

### 2.4. Characterization

**2.4.1. Chemical structure of T-CNT.** The functional groups of the surface-modified CNT (T-CNT) were confirmed by Fourier transform-infrared spectroscopy (FT-IR, Frontier<sup>TM</sup>, Perkin Elmer, Inc., USA) in transmission mode. The CNT was mixed with KBr powder, then ground and compressed to make a pellet for FT-IR. Energy dispersive X-ray spectrometry (EDS) coupled with a field emission scanning electron microscope

(FE-SEM, SUPRA 40VP, Carl Zeiss, Inc., Germany) was used to monitor the morphology and chemical composition.

**2.4.2. Cure characteristics.** The crosslinking characteristics of the SBR compounds were evaluated in terms of maximum torque ( $M_H$ ), minimum torque ( $M_L$ ), scorch time ( $T_{s2}$ ), optimum cure time ( $T_{90}$ ), and cure rate index (CRI) at 170  $^{\circ}\text{C}$  for 30 min using an oscillating disk rheometer (ODR 2000, Alpha Technologies, USA).

**2.4.3. Abrasion behavior.** A schematic diagram of the blade abrader is given in Fig. 2.<sup>38–40</sup> In this setup, a cylindrical rubber disk is held in an aluminum backing plate. The rubber disk was 38 mm in diameter and 10 mm in height, with a central hole, measuring 12.5 mm in diameter. The aluminum backing plate, 38 mm in diameter and about 6 mm thick, was mounted in a lathe chuck and rotated about its axis at 10 rev per min. A zirconia blade (sdf5, Ruifengli Blade Manufacturing Co. Ltd, China) was held in a clamp attached to a stationary compound slide table. The blade shaft can be advanced horizontally in controlled increments, allowing the blade to be pressed against the flat surface of the rotating rubber disk. The torque experienced on the blade shaft, generated by the frictional rotation of the rubber disk, was measured and subsequently converted into the corresponding frictional energy input,  $W_f$ . The detailed description of the experimental procedure is provided elsewhere.<sup>40</sup> The rate of wear was determined after the wear pattern, typically called the “Schallamach pattern”, was fully developed. The loss in height of the rubber disk was measured precisely using the position sensor of the blade shaft and expressed as  $R_h$  (mm rev<sup>-1</sup>). Previous studies have established that the weight loss is closely proportional to height loss.<sup>40</sup> Furthermore, it has been reported that a power-law relation exists between  $R_h$  and  $W_f$ , as expressed in eqn (1);<sup>41</sup>

$$R_h = kW_f^n \quad (1)$$

where  $k$  is a constant and  $n$  is the power-law exponent.

**2.4.4. Crack growth behavior.** The rate of crack growth,  $dc/dn$ , defined as the crack increment per cycle of straining, is given by the following power-law relationship as shown in eqn (2);<sup>41</sup>

$$\frac{dc}{dn} = k'G^n \quad (2)$$

Table 1 Formulation of SBR compounds (unit: phr)

Materials	CB50	CB49/ CNT1	CB47/ CNT3	CB49/ T-CNT1	CB47/ T-CNT3
SBR	100	100	100	100	100
CB	50	49	47	49	47
p-CNT	—	1	3	—	—
T-CNT	—	—	—	1	3
ZnO	3	3	3	3	3
S/A	1	1	1	1	1
Irganox 1010	1	1	1	1	1
NS	1	1	1	1	1
S	2	2	2	2	2

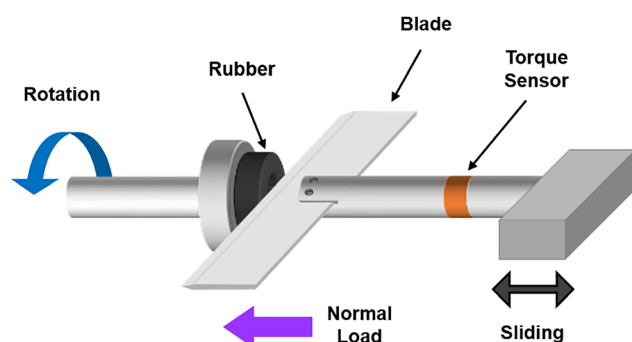


Fig. 2 Sketch of blade abrader.<sup>38–40</sup>



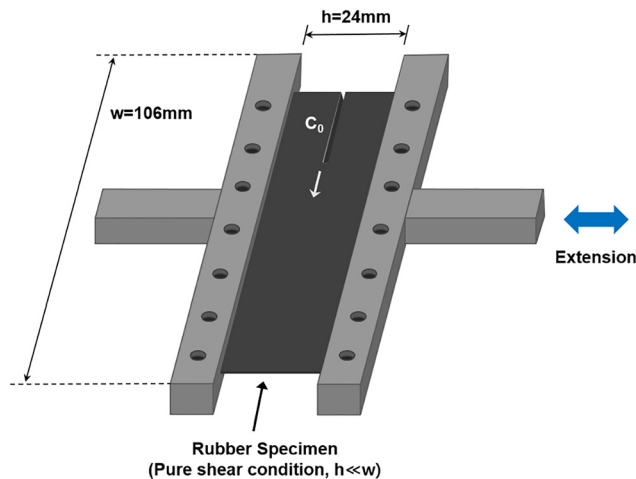


Fig. 3 Sketch of the crack growth experiment under pure shear conditions.<sup>41</sup>

where  $G$  is the tearing energy,  $k'$  is a constant, and  $n'$  is the power-law exponent. The experimental setup for the crack growth test under pure shear conditions is illustrated in Fig. 3. The rubber specimen had dimensions of width,  $w = 106$  mm, clamping length,  $h = 24$  mm, and thickness,  $t = 2$  mm. An initial pre-cut of  $c_0 = 40$  mm was introduced, and the subsequent crack length,  $c$  was measured at intervals of 500 cycles using a zoom camera fixed at a constant position. The rate of crack growth was determined from the average slope of the plot of propagated crack length  $c$  versus number of cycles  $n$ . The applied strain was varied up to approximately 0.2.

**2.4.5. Morphology of fracture surfaces.** The morphology of the fracture surfaces resulting from abrasion and crack propagation was observed using a field-emission electron scanning microscope (FE-SEM, SUPRA40VP, Carl Zeiss, Germany) operating at accelerating voltages of 2 and 15 kV.

## 3. Results and discussion

### 3.1. Chemical structure of T-CNT

Fig. 4 shows the FT-IR spectra of the pristine (p-CNT) and treated CNT (T-CNT). The C=C and C-H stretchings were observed peaks at  $1550\text{ cm}^{-1}$  and  $3000\text{ cm}^{-1}$  for both p-CNT and T-CNT. The strong O-H stretching peaks were observed at  $3200\text{--}3650\text{ cm}^{-1}$  for T-CNT, possibly due to the strong acid treatment. Moreover, the characteristic Si-O and S-S stretching peaks were observed at  $800$  and  $550\text{ cm}^{-1}$  for T-CNT, suggesting clear evidence for the Si-69 treatment. The presence of elements, Si and S, in T-CNT was also proved by EDS analysis, as shown in Fig. 5.

### 3.2. Cure characteristics

The crosslinking characteristics of the SBR compound are shown in Table 2. When a small amount of CB was replaced by the CNT, the apparent crosslinking density ( $\Delta M$ ) tended to decrease. This is thought to be due to the decrease in the bound rubber formed between CB and SBR. Since sulfur with a

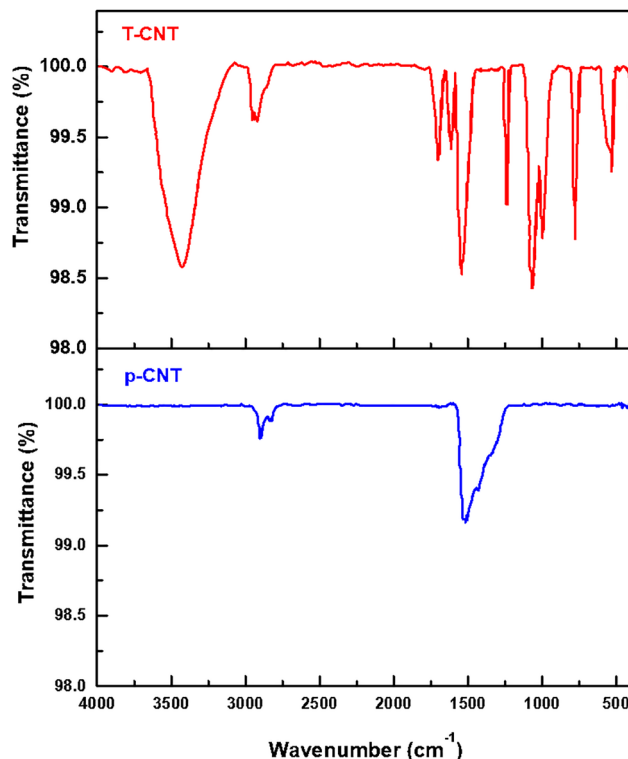


Fig. 4 FT-IR spectra of p-CNT and T-CNT.

relatively large atomic size cannot penetrate the bound rubber layer with a high rubber chain density, the higher the amount of bound rubber, the higher the proportion of sulfur present in the rubber matrix, which results in a higher crosslinking density.<sup>42,43</sup> However, since the CNT has poorer bonding interactions with rubber than with CB, less bound rubber is formed between the CNT and SBR.<sup>44</sup> Therefore, it is thought that the apparent crosslinking density decreased due to the decrease in bound rubber when CB was replaced with a small amount of CNT. The scorch time ( $T_{s2}$ ) and optimal crosslinking time ( $T_{90}$ ) decreased, and the cure rate index (CRI) increased when a portion of CB was replaced with the CNT. This behavior is attributed to the high thermal conductivity and large specific surface area of CNTs, which promote more uniform heat distribution within the rubber compound and a faster increase in local temperature during the crosslinking reaction.<sup>45</sup> This effect became even more pronounced when surface-modified CNTs were used. These CNTs are functionalized with a silane coupling agent on their surfaces, which can be confirmed from the slightly roughened appearance of the modified-CNT surfaces observed in FE-SEM images.<sup>46</sup> The silane coupling agent on the CNT surface chemically bonds with the rubber matrix, enhancing rubber-filler interactions.

### 3.3. Effect of CNTs on wear behavior

The wear rate ( $R_w$ ) of the SBR compounds was evaluated using a blade-type wear tester and is plotted as a function of the frictional energy input ( $W_f$ ) on a log-log scale (Fig. 6). A linear relationship was found for all rubber compounds, confirming



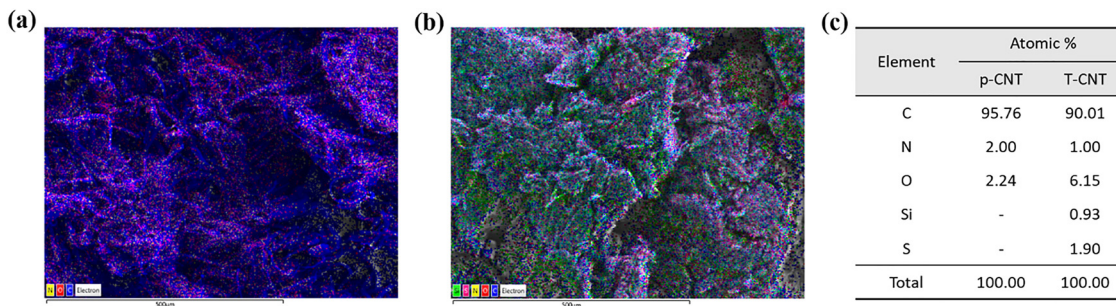


Fig. 5 EDS image of (a) p-CNT and (b) T-CNT, and (c) atomic percentage.

Table 2 Cure characteristics of SBR compounds

	$M_H$ (Nm)	$M_L$ (Nm)	$\Delta M$ (Nm)	$T_{S2}$ (min)	$T_{90}$ (min)	CRI <sup>a</sup>
CB50	4.42	1.16	3.26	4.68	12.08	13.50
CB49/CNT1	4.26	1.92	2.34	4.20	8.98	20.91
CB47/CNT3	4.41	1.80	2.61	4.43	9.67	19.11
CB49/T-CNT1	4.13	1.48	2.65	3.27	8.42	19.42
CB47/T-CNT3	4.45	1.85	2.60	3.37	8.53	19.38

<sup>a</sup> CRI (cure rate index):  $100/(T_{90} - T_{S2})$ .

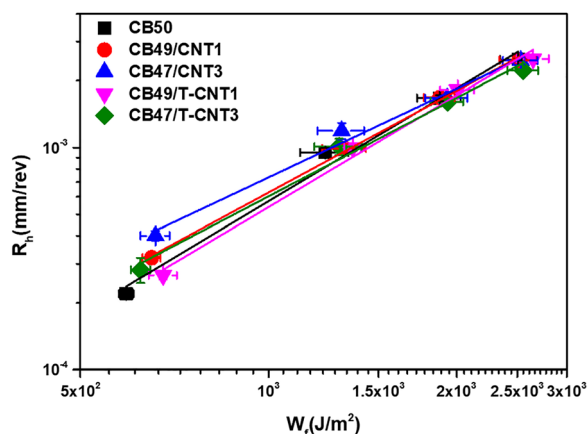


Fig. 6 Wear rate,  $R_h$ , as a function of frictional energy,  $W_f$ , for SBR composites.

typical 'power-law' dependence, as expected in eqn (1). When CB was partially replaced with a small amount of unmodified CNT, the overall wear resistance tended to decrease. However, the replacement with the surface-modified CNT resulted in a marginal improvement in wear performance. To elucidate the underlying mechanism, the worn surfaces were examined, as shown in Fig. 7. For all SBR compounds, a typical Schallamach pattern composed of regularly spaced ridges was observed.<sup>39,40,47</sup> This suggests that abrasion proceeds predominantly through the accumulated crack propagation at the base of ridges. When CB was replaced by the unmodified CNT (Fig. 7(b) and (c)), distinct CNT accumulation was evident within the ridge tongue regions. This is because unmodified CNTs are more easily pulled out of the rubber matrix by the blade during wear and subsequently accumulate in the ridge areas, as schematically given in Fig. 8(a).

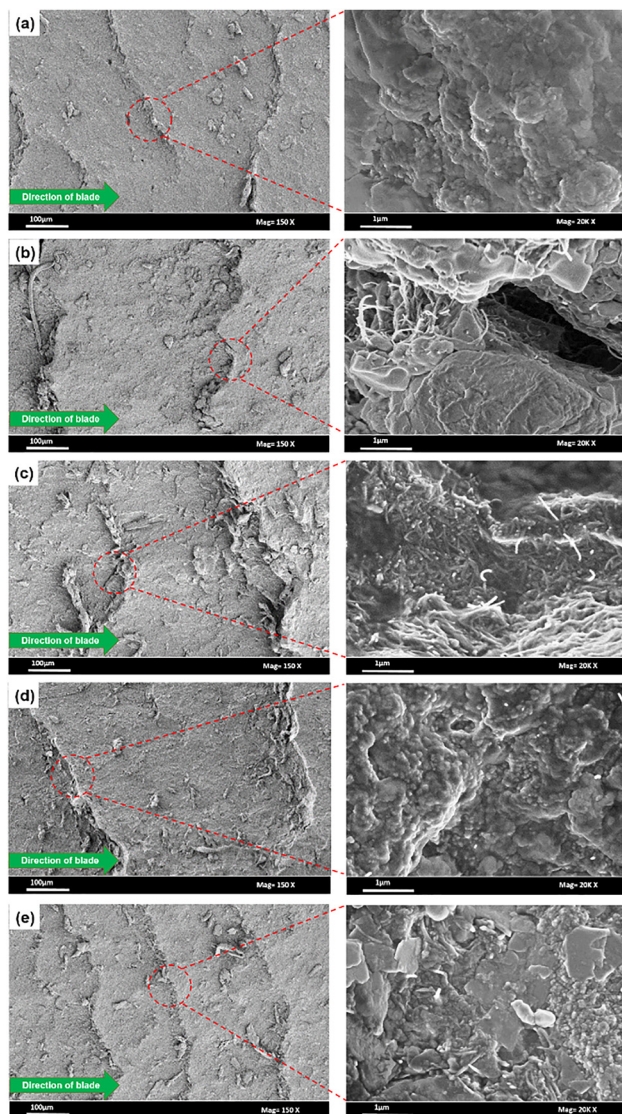


Fig. 7 FE-SEM images of the worn surface for (a) CB50, (b) CB49/CNT1, (c) CB47/CNT3, (d) CB49/T-CNT1, and (e) CB47/T-CNT3.

This behavior is consistent with previous reports on the weak interfacial interactions between the untreated CNT and rubber matrices.<sup>48,49</sup> Such aggregation appears to contribute directly to the deterioration of the wear performance. As the unmodified



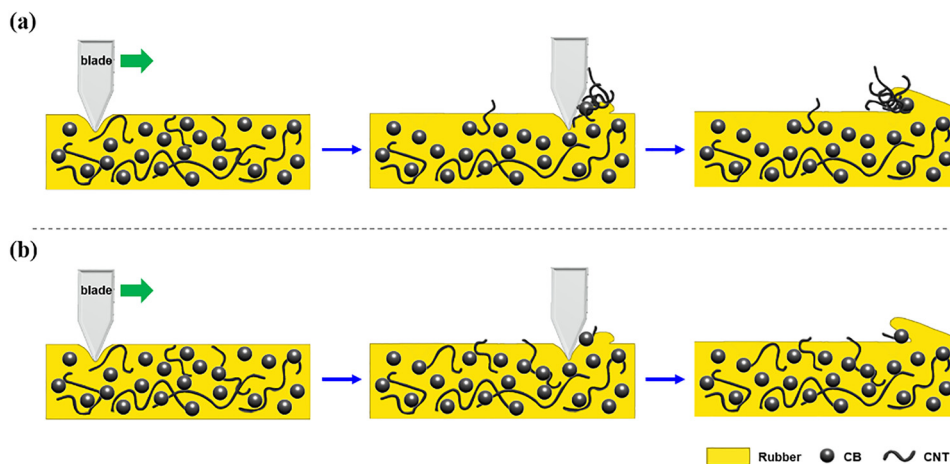


Fig. 8 Schematic representation of the abrasion behavior of SBR composites with (a) p-CNT and (b) T-CNT.

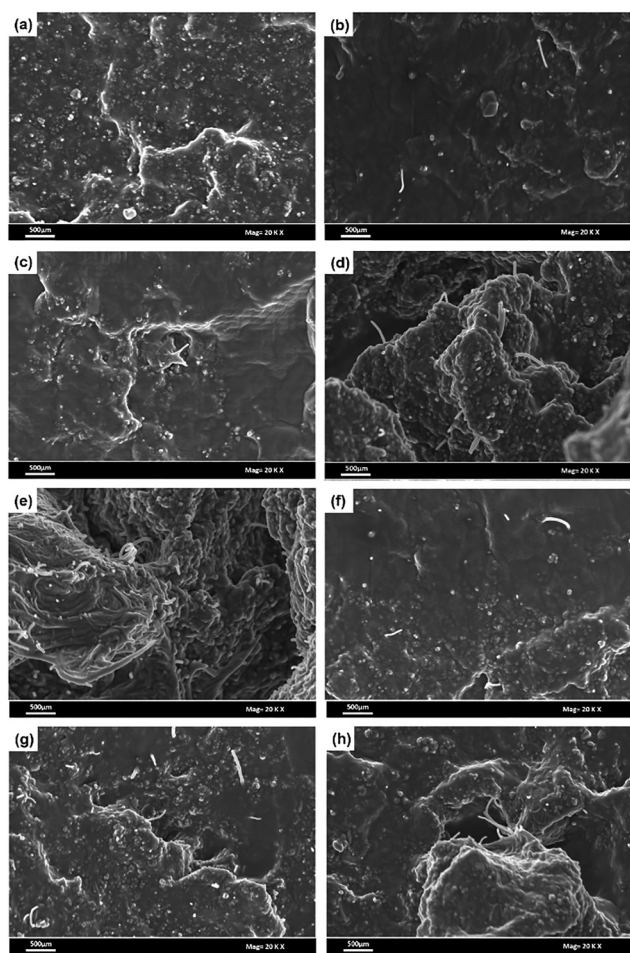


Fig. 9 FE-SEM images of the cross-sectional surfaces of the SBR composites before wear: (a) CB50, (b) and (c) CB49/CNT1, (d) and (e) CB47/CNT3, (f) CB49/T-CNT1, and (g) and (h) CB47/T-CNT3.

CNT content increased, the dispersion became poorer and a higher degree of CNT aggregation was observed (Fig. 9(c) and (e)) in the SBR composite, facilitating the detachment of

CNTs from the rubber matrix under the movement of the blade. As a result, a larger amount of CNT accumulation was observed in the ridge area, ultimately causing a further decline in the wear performance.

On the other hand, the worn surface of the SBR composite containing 1 phr of the surface-modified CNT (Fig. 7(d)) displayed a significantly reduced level of CNT accumulation in the ridge regions. This can be attributed to the stronger interfacial bonding between the CNT and SBR induced by surface modification, which effectively suppressed CNT pull-out during wear and consequently improved wear resistance. The wear resistance of CB49/T-CNT1 increased from 6 to 7.5% compared to CB50 when the frictional energy was increased from 0.7 to 2.5  $\text{kJ m}^{-2}$ . As the surface-modified CNT loading was further increased, dispersion became less effective, and CNTs tended to agglomerate (Fig. 9(h)). Consequently, a slight increase in CNT accumulation was observed in the ridge area (Fig. 7(e)), resulting in a reduction in wear performance. However, at the higher frictional energy level (2.5  $\text{kJ m}^{-2}$ ), CB47/T-CNT3 exhibited the best wear performance, showing a 13.8% improvement in wear resistance compared to CB50. This might be explained by the higher mechanical strength due to the higher T-CNT reinforcement, which can compensate for the negative effect on wear caused by the agglomeration of T-CNTs.

The cross-link density of rubber is also one of the key factors significantly affecting the abrasion performance. In general, a higher cross-link density leads to an improved wear resistance.<sup>50</sup> CB50 with the highest crosslink density showed a better wear resistance compared to CB49/CNT1, CB47/CNT3, and CB47/T-CNT3 at the lower frictional energy ( $W_f$ ) region, and this trend became opposite as the  $W_f$  was increased. This indicates that the wear rate of CB50 is more sensitive to the wear severity ( $W_r$ ) (see Table 3). It has been reported that the more elastic compounds generally show a higher slope in such a plot between  $R_h$  and  $W_f$ .<sup>40</sup> The lower sensitivity of CNT-containing compounds in this study could be explained by the findings on higher hysteresis losses for CNT-containing rubber compounds upon mechanical deformation.<sup>48,49</sup>



**Table 3** Linear fitting parameters of wear ( $n$ ,  $k$ ) and crack growth ( $n'$ ,  $k'$ ) behaviors for SBR composites ( $n$  and  $n'$ : slope,  $k$  and  $k'$ : intercept)

	CB50	CB49/CNT1	CB47/CNT3	CB49/T-CNT1	CB47/T-CNT3
$K$	-8.29	-7.77	-7.12	-8.28	-7.64
$N$	1.68	1.52	1.33	1.67	1.47
$k'$	-5.98	-6.31	-6.32	-6.36	-6.82
$n'$	2.12	1.88	1.19	2.14	1.31

### 3.4. Effect of CNTs on crack growth behavior

The crack growth rate ( $dc/dn$ ) as a function of tear energy ( $G$ ) is presented in Fig. 10. A linear relationship was found for all compounds, indicating 'power-law' dependence between  $dc/dn$  and  $G$ , as shown in eqn (2).<sup>41</sup> When CB was partially replaced with a small amount of CNT, the overall rate of crack growth decreased, and the fatigue resistance of the composite improved. This effect was even greater in the case of the surface-modified CNT. In the range of tearing energy  $G$  from 0.3 to 0.7  $\text{kJ m}^{-2}$ , the fatigue resistance of CNT-replaced compounds was enhanced: 70–71.8% for CB47/T-CNT3, 39.8–62.5% for CB49/T-CNT1, 25.4–60.6% for CB49/CNT1, and 7.1–11.5% for CB47/CNT3, compared to that of CB50. Owing to their fibrous morphology and high aspect ratio, CNTs are more effective than spherical CB particles in delaying crack growth, thereby enhancing fatigue resistance.

The fatigue fracture surface of the SBR compound with only CB (Fig. 11(a)) exhibited typical features of a reinforced system, with CB particles uniformly dispersed within the SBR matrix and a rough fracture surface. However, when CB was substituted with CNTs (Fig. 11(b)–(f)), some of the fibrous CNTs were observed protruding from the SBR sheet. These CNTs were often oriented perpendicular to the crack growth direction, suggesting that they acted as physical barriers to crack growth before being pulled out during cyclic deformation. Such morphological characteristics and the alignment of CNTs appear to contribute significantly to the improvement of fatigue resistance in CB/CNT-filled SBR.

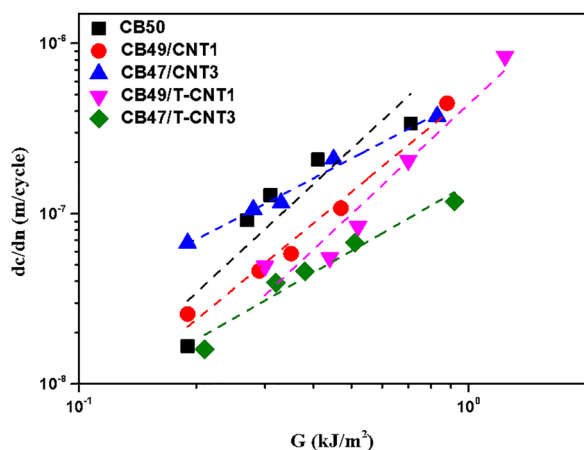


**Fig. 10** Crack growth rate,  $dc/dn$ , as a function of tear energy,  $G$ , for SBR composites.

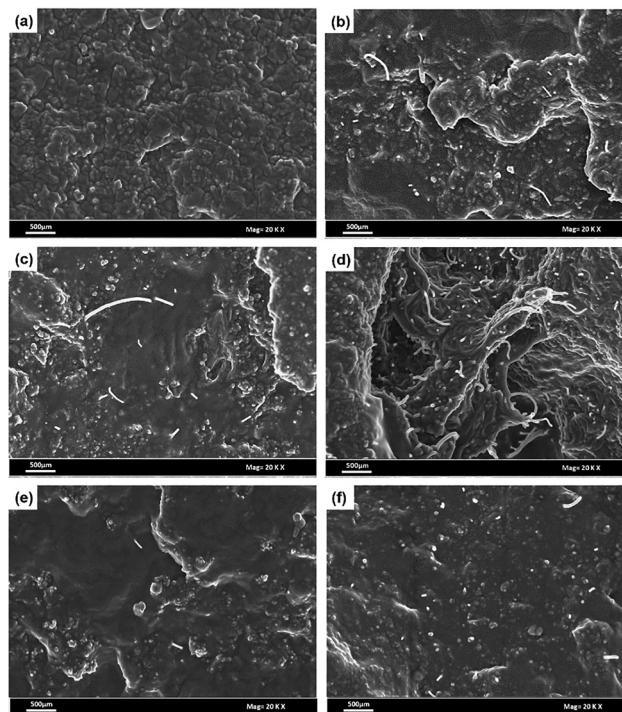


**Fig. 11** FE-SEM images of the fatigue fractured surface for (a) CB50, (b) CB49/CNT1, (c) and (d) CB47/CNT3, (e) CB49/T-CNT1, and (f) CB47/T-CNT3.

In the case of the unmodified CNT (Fig. 11(b)–(d)), the CNTs were generally pulled out in long, continuous fibers, reflecting weak interfacial adhesion between the CNT and the rubber matrix. As the CNT content increased to 3 phr, poor dispersion was also observed, resulting in the formation of CNT aggregates (Fig. 9(e)). Since these CNT clusters are more easily pulled out of the rubber matrix, the crack growth rate increased, and the rubber matrix displayed deep indentations caused by the protrusion of CNT clusters (Fig. 11(d)).

On the other hand, the fracture surfaces of compounds containing modified CNTs (Fig. 11(e) and (f)) exhibited shorter pulled-out CNTs, indicative of stronger bonding and improved dispersion within the matrix. As a result, fatigue resistance was further enhanced with increasing loadings of surface-modified CNTs. Based on these morphological analyses of fatigue fracture surfaces, the mechanisms of fatigue failure for SBR containing unmodified and surface-modified CNTs are schematically shown in Fig. 12.

The rate of crack growth is also affected by the cross-link density. In general, an increase in cross-link density reduces the crack growth rate; however, once it exceeds a certain critical level, the rate begins to increase again.<sup>51</sup> In the lower tear energy ( $G$ ) region, CB50, which exhibited the highest apparent cross-link density ( $\Delta M$ ), showed a lower crack growth rate than the SBR compounds containing unmodified CNTs and was comparable with the compounds having modified CNTs. The rate of crack growth for CB50 increased sharply with increasing tearing energy  $G$  (see Table 3), and it generally showed a higher rate of crack growth than rubber compounds with CNTs, having



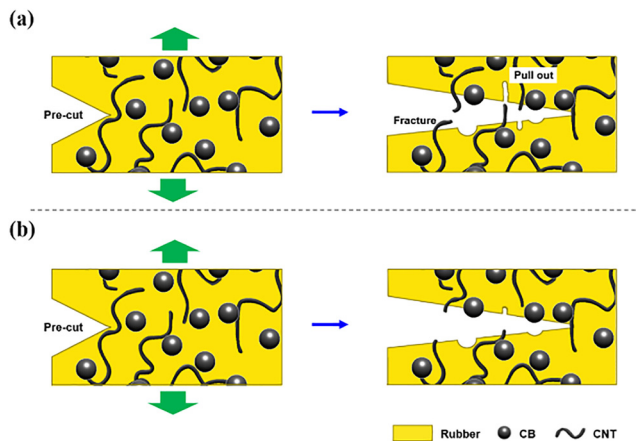


Fig. 12 Schematic representation of the crack growth behaviors of SBR composites with (a) p-CNT and (b) T-CNT.

higher hysteresis losses upon deformation, which is very similar behavior of the wear mentioned above.

### 3.5. Correlation between abrasion and crack growth

When repeated friction is applied to a rubber material, ridges are formed perpendicular to the sliding direction. Wear then occurs as a continuous frictional force acting on the ridge tongue. This process resembles the crack growth mechanism, in which cracks gradually propagate under repeated deformation. Previous studies have shown a close correlation between friction–wear characteristics and crack growth behavior.<sup>41,52,53</sup> To verify this relationship, the wear ( $R_h$  vs.  $W_f$ ) and crack growth ( $dc/dn$  vs.  $G$ ) behaviors are plotted on the same scale as shown in Fig. 13. The linear fitting parameters for wear ( $n$  and  $k$ ) and crack growth ( $n'$  and  $k'$ ) are summarized in Table 3, where  $n$  and  $n'$  represent the slopes and  $k$  and  $k'$  represent the intercepts of the respective behaviors. The results revealed a strong correspondence between wear and fatigue fracture, with both

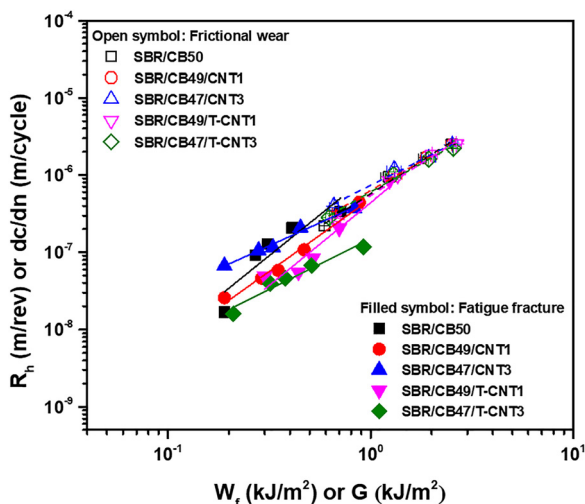


Fig. 13 Correlation between abrasion ( $R_h$  vs.  $W_f$ ) and crack growth ( $dc/dn$  vs.  $G$ ) behaviors for SBR composites.

exhibiting similar slopes and energy distributions. These findings confirm that the SBR containing CB and CNTs follows a typical wear mechanism in which frictional wear is governed by crack growth processes.

## 4. Conclusions

In this study, the wear and fatigue fracture characteristics of CB-filled SBR composites were evaluated with respect to the CNT content and surface modification. The CNT was surface-modified using acid treatment and a silane coupling agent (Si-69) and incorporated into the SBR by partially replacing CB with a small amount of CNT, based on a reference loading of 50 phr CB. The wear rate ( $R_h$ ) and crack growth rate ( $dc/dn$ ) of the CB/CNT-filled SBR showed a power-law relationship with the friction energy ( $W_f$ ) and tear energy ( $G$ ), respectively. When CB was replaced with the unmodified CNT, wear resistance decreased as the unmodified CNT was easily pulled out of the SBR matrix during the wear process. However, when 1 phr of the surface-modified CNT was introduced, the interfacial bonding between the CNT and the SBR matrix increased, resulting in reduced CNT pull-out and markedly improved wear resistance (6–7.5% higher than CB50). Regarding fatigue fracture characteristics, the incorporation of CNTs contributed to enhanced fatigue resistance (7.08–60.6% higher than CB50) due to their elongated fibrous morphology. Furthermore, surface-modified CNTs provided superior fatigue resistance (39.8–71.8% higher than CB50) compared with unmodified CNT, as stronger interfacial interactions with the SBR matrix inhibited crack propagation. These findings suggest that effective surface treatment of CNTs is essential when targeting improved wear performance in tire tread compounds. Additionally, CNTs demonstrate strong potential as reinforcing fillers in tire components that require enhanced crack growth resistance, such as belt cushion compounds.

## Conflicts of interest

There are no conflicts to declare.

## Data availability

No primary research results, software or code have been included, and no new data were generated or analysed as part of this review.

Supplementary information (SI) is available. See DOI: <https://doi.org/10.1039/d5ma01175b>.

## Acknowledgements

This work was funded by research support from Jeonbuk National University in 2024. This work was also partially supported by the Technology Innovation Program (20010851, Advanced Butadiene Rubber and Functional Complex Development for Super Abrasion



Tires) funded by the Ministry of Trade, Industry & Energy (MOTIE, Korea).

## References

- 1 T. Kurian and N. M. Mathew, Natural Rubber: Production, Properties and Applications, in *Biopolymers: Biomedical and Environmental Applications*, ed. S. Kalia and L. Avérous, Scrivener Publishing LLC, Beverly, 2011, pp. 403–436.
- 2 C. M. Bhuvaneshwari, S. S. Kale, G. Gouda, P. Jayapal and K. Tamilmani, Elastomers and Adhesives for Aerospace Applications, in *Aerospace Materials and Material Technologies*, ed. N. Prasad and R. Wanhill, *Indian Institute of Metals Series*, Springer, Singapore, 2017, pp. 563–586.
- 3 Custom Market Insights, Global Rubber Compound Market 2024-2033 (Report Code CMI45303), Custom Market Insights (2024).
- 4 A. Ansari, T. R. Mohanty, S. Sarkar, S. Ramakrishnan, S. K. P. Amarnath and N. K. Singha, Epoxy Modified Styrene Butadiene Rubber (SBR) in Green Tire Application, *Eur. Polym. J.*, 2024, **213**, 113069.
- 5 R. J. Dhanorkar, S. Mohanty and V. K. Gupta, Synthesis of Functionalized Styrene Butadiene Rubber and Its Applications in SBR–Silica Composites for High Performance Tire Applications, *Ind. Eng. Chem. Res.*, 2021, **60**, 4517.
- 6 H. Colvin, General-Purpose Elastomers, in *Rubber Compounding: Chemistry and Applications*, ed. B. Rodgers, Marcel Dekker, New York, 2004, pp. 33–82.
- 7 P. Sae-oui, K. Suchiva, C. Sirisinha, W. Intiya, P. Yodjun and U. Thepsuwan, Effects of Blend Ratio and SBR Type on Properties of Carbon Black-Filled and Silica-Filled SBR/BR Tire Tread Compounds, *Adv. Mater. Sci. Eng.*, 2017, **2017**, 2476101.
- 8 G.-Y. Um, T. Kwon, S. H. Lee, W. Kim, J. Kim, H. J. Kim and J. H. Lee, The Influence of Styrene Content in Solution Styrene Butadiene Rubber on Silica-Filled Tire Tread Compounds, *Polymers*, 2023, **15**, 4288.
- 9 S. Bulbul and M. E. Ergun, Effect of Mica Powder-Filled Styrene-Butadiene Rubber Compounds on Crosslink Density and Mechanical Properties, *Therm. Sci.*, 2022, **26**, 3019.
- 10 S. H. Song, Influence of Eco-Friendly Processing Aids on Silica-Based Rubber Composites, *Appl. Sci.*, 2020, **10**, 7244.
- 11 G. W. Jo and D. H. Lee, Wear of Rubber, *Elastomers Compos.*, 1995, **30**, 247.
- 12 B. B. Boonstra, Role of Particulate Fillers in Elastomer Reinforcement: A Review, *Polymer*, 1979, **20**, 691.
- 13 M. J. Wang, P. Zhang and K. Mahmud, Carbon-Silica Dual Phase Filler, a New Generation Reinforcing Agent for Rubber: Part IX. Application to Truck Tire Tread Compound, *Rubber Chem. Technol.*, 2001, **74**, 124.
- 14 G. Thielen, Chemically Modified Eulsion SBR in Tire Treads, *Rubber Chem. Technol.*, 2008, **81**, 625.
- 15 K. Kim, J.-Y. Lee, B.-J. Choi, B. Seo, G.-H. Kwag, H.-J. Paik and W. Kim, Styrene-Butadiene-Glycidyl Methacrylate Terpolymer/Silica Composites: Dispersion of Silica Particles and Dynamic Mechanical Properties, *Compos. Interfaces*, 2014, **21**, 685.
- 16 B. Seo, H. Kim, H. Paik, G. Kwag and W. Kim, Characterization of AN-SBR/silica compound with acrylonitrile as a polar group in SBR, *Macromol. Res.*, 2013, **21**, 738.
- 17 N. Torbati-Fard, S. M. Hosseini and M. Razzaghi-Kashani, Effect of The Silica-Rubber Interface on The Mechanical, Viscoelastic, and Tribological Behaviors of Filled Styrene-Butadiene Rubber Vulcanizates, *Polym. J.*, 2020, **52**, 1223.
- 18 J. Liang, Y. Liu, X. Lv, Y. Chen, Y. Chen and L. Liu, Enhancing Mechanical Properties of Rubber Composites via Hydroxylation and Silane Coupling of Carbon Black, *J. Appl. Polym. Sci.*, 2025, **142**, e57516.
- 19 L. Wang, Z. Luo, L. Yang, J. Zhong and Y. Xu, Synergistic Effect of Styrene and Carbon Black on the Fatigue Properties of Styrene-Butadiene Rubber Composites, *ACS Omega*, 2024, **9**, 2000.
- 20 P. Thaptong, P. Sae-Oui, P. Jittham and C. Sirisinha, Optimization of Highly Dispersible Silica/Carbon Black Hybrid Filler Ratio for Tire Tread Based on Solution- and Emulsion-Styrene Butadiene Rubber, *J. Appl. Polym. Sci.*, 2022, **139**, e52608.
- 21 A. Mazumder, J. Chanda, S. Bhattacharyya, S. Dasgupta, R. Mukhopadhyay and A. K. Bhowmick, Improved Tire Tread Compounds Using Functionalized Styrene Butadiene Rubber-Silica Filler/Hybrid Filler Systems, *J. Appl. Polym. Sci.*, 2021, e51236.
- 22 T. Dolui, J. Chanda, P. Ghosh, R. Mukhopadhyay and S. S. Banerjee, Synergistic Effect of Hybrid Filler Networks on Morphology and Enhanced Properties of Hydrogenated Styrene Butadiene Rubber for Tyre Tread Application, *J. Polym. Res.*, 2025, **32**, 213.
- 23 L. Yin, Z. Luo, J. Zhong, B. Yang and Y. Ji, Behaviour and Mechanism of Fatigue Crack Growth in Aramid-Fibre-Reinforced Styrene-Butadiene Rubber Composites, *Int. J. Fatigue*, 2020, **134**, 105502.
- 24 M. Kodal, N. Y. Çakır, R. Yıldırım, N. Karakaya and G. Özkoç, Improved Heat Dissipation of NR/SBR-Based Tire Tread Compounds via Hybrid Fillers of Multi-Walled Carbon Nanotube and Carbon Black, *Polymers*, 2023, **15**, 4503.
- 25 M. A. Rhue, B. Lassley, C. Bavluka, S. Crossley and B. P. Grady, Mechanochemical Sulfur Functionalization of Carbon Nanotubes for Partial Replacement of Carbon Black in Tire Tread Rubber, *J. Polym. Sci.*, 2025, **1**, DOI: [10.1002/pol.20250971](https://doi.org/10.1002/pol.20250971).
- 26 R. Xu, W. Sheng, F. Zhou and B. N. J. Persson, Rubber Wear: History, Mechanisms, and Perspectives, *Tribol. Lett.*, 2025, **73**, 90.
- 27 A. H. Muhr and A. D. Roberts, Rubber Abrasion and Wear, *Wear*, 1992, **158**, 213.
- 28 R. Stoczek, G. Heinrich, R. Kipscholl and O. Kratina, Cut & Chip Wear of Rubbers in A Range from Low up to High Severity Conditions, *Appl. Surf. Sci. Adv.*, 2021, **6**, 100152.
- 29 J. H. Go and C. Nah, Wear of Rubber for Tire, *Polym. Sci. Technol.*, 1995, **6**, 348.
- 30 E. Chae, S. R. Yang, S. H. Cho and S.-S. Choi, Influence of Dicyclopentadiene Resin on Abrasion Behavior of Silica-



- Filled SBR Compounds Using Different Abrasion Testers, *Elastomers Compos.*, 2023, **58**, 103.
- 31 M. Heinz, A Universal Method to Predict Wet Traction Behaviour of Tire Tread Compounds in The Laboratory, *J. Rubber Res.*, 2010, **13**, 91.
- 32 K. A. Grosch, Correlation between Road Wear of Tires and Computer Road Wear Simulation using Laboratory Abrasion Data, *Rubber Chem. Technol.*, 2004, **77**, 791.
- 33 N. Andre, G. Cailletaud and R. Piques, Haigh Diagram for Fatigue Crack Initiation Prediction of Natural Rubber Components, *Kautsch. Gummi Kunstst.*, 1999, **52**, 120.
- 34 C. Champy, V. L. Saux, Y. Marco, T. Glanowski, P. Charrier and W. Hervouet, Fatigue of Crystallizable Rubber: Generation of A Haigh Diagram Over A Wide Range of Positive Load Ratios, *Int. J. Fatigue*, 2021, **150**, 106313.
- 35 D. W. Lee, S. R. Kim, K. D. Sung, J. S. Park, T. W. Lee and S. C. Huh, A Study on The Fatigue Life Prediction of Tire Belt-layers Using Probabilistic Method, *J. Mech. Sci. Technol.*, 2013, **27**, 673.
- 36 R. J. Harbour, A. Fatemi and W. V. Mars, Fatigue Crack Growth of Filled Rubber under Constant and Variable Amplitude Loading Conditions, *Fatigue Fract. Eng. Mater. Struct.*, 2007, **30**, 640.
- 37 W. V. Mars and A. Fatemi, A Literature Survey on Fatigue Analysis Approaches for Rubber, *Int. J. Fatigue*, 2002, **24**, 949.
- 38 G.-B. Lee, D. Kim, S. Lee, S. Kim, M.-S. Ahn, B. Mensah and C. Nah, Wear Behavior of Silica filled Styrene-Butadiene Rubber: A Comparative Study Between the Blade-Type and Akron-Type Abrader, *Elastomers Compos.*, 2023, **58**, 179.
- 39 A. N. Gent and C. Nah, Abrasion of rubber by a blade abrader: Effect of blade sharpness and test temperature for selected compounds, *Rubber Chem. Technol.*, 1996, **69**, 819.
- 40 C. Nah, PhD Dissertation, Wear Mechanisms of Rubber Compounds, The University of Akron, USA, 1995.
- 41 M. D. Ellul, Mechanical Fatigue, in *Engineering with Rubber: How to Design Rubber Components*, ed. A. N. Gent, Hanser, Munich, 2012, pp. 159–203.
- 42 S. Lee and N. C. Park, Studies on the Crosslinking Density and Reinforcement of Rubber Compounds by Cure System, *Elastomer*, 1998, **33**, 315.
- 43 S.-S. Choi, K.-J. Hwang and B.-T. Kim, Influence of Bound Polymer on Cure Characteristics of Natural Rubber Compounds Reinforced with Different Types of Carbon Blacks, *J. Appl. Polym. Sci.*, 2005, **98**, 2282.
- 44 B. Mensah, H. G. Kim, J.-H. Lee, S. Arepalli and C. Nah, Carbon Nanotube-reinforced Elastomeric Nanocomposites: A Review, *Int. J. Smart Nano Mater.*, 2016, **6**, 211.
- 45 S. Makhno, X. Wan, O. Lisova, P. Gorbyk, D. Wang, H. Tang, Y. Shi, M. Kartel, K. Ivanenko, S. Hozhdzinskyi, G. Zaitseva, M. Stetsenko and Y. Sementsov, Conducting Rubber Anisotropy of Electrophysical and Mechanical Properties, *Polymers*, 2025, **17**, 492.
- 46 Y. Nakaramontri, C. Kummerlowe, C. Nakason and N. T. Vennemann, The Effect of Surface Functionalization of Carbon Nanotubes on Properties of Natural Rubber/Carbon Nanotube Composites, *Polym. Compos.*, 2015, **36**, 2113.
- 47 A. N. Gent and C. T. R. Pulford, Mechanisms of Rubber Abrasion, *J. Appl. Polym. Sci.*, 1983, **28**, 943.
- 48 C. Nah, J. Y. Lim, B. H. Cho, C. K. Hong and A. N. Gent, Reinforcing Rubber with Carbon Nanotubes, *J. Appl. Polym. Sci.*, 2010, **118**, 1574.
- 49 C. Nah, J. Y. Lim, R. SenGupta, B. H. Cho and A. N. Gent, Slipping of Carbon Nanotubes in A Rubber Matrix, *Polym. Int.*, 2011, **60**, 42.
- 50 K. Cho and D. Lee, Effect of Molecular Weight Between Cross-links on The Abrasion Behavior of Rubber by A Blade Abrader, *Polymer*, 2000, **41**, 133.
- 51 G. R. Hamed and N. Rattanasom, Effect of Crosslink Density on Cut Growth in Gum Natural Rubber Vulcanizates, *Rubber Chem. Technol.*, 2002, **75**, 323.
- 52 H. Lee, W. Wang, B. Shin, S. L. Kang, K. C. Gupta and C. Nah, A Correlation between Crack Growth and Abrasion for Selected Rubber Compounds, *Elastomers Compos.*, 2019, **54**, 313.
- 53 D. H. Champ, E. Southern and A. G. Thomas, Fracture Mechanics Applied to Rubber Abrasion, in *Advances in Polymer Friction and Wear*, ed. L.-H. Lee, Plenum Press, New York, 1974, pp. 133–144.

